Robust Direct Current Control of Single-Phase PWM Rectifiers Based on a Mixed H_2/H_∞ Controller

Motaz Musa IBRAHIM, Lei MA*, Yiming ZHAO, Haoran LIU
Southwest Jiaotong University, Xipu, Chengdu, 611756, China
mootaz99@hotmail.com, malei@swjtu.edu.cn (**Corresponding author*)

Abstract: Robustness for single-phase pulse-width modulation (PWM) rectifiers which are employed for electric locomotives is essential since a train works in a dynamic environment where faults such as parameter perturbations and measurement errors often occur. These faults may lead to a subsequent failure and damage of costly components; thus, robust control is highly recommended. Apart from the robustness of a rectifier, its dynamic performance should also be considered. This paper presents the implementation of a direct current control (DCC)-based mixed H_2/H_∞ controller for single-phase PWM rectifiers with the purpose of achieving robustness and a decent dynamic response in the presence of inductance variation, where settling time and percentage overshoot can be addressed by means of the pole placement method. In addition, the ν-gap metric has been used as a tool for estimating robust stability. The proposed controller is compared with the direct current control-based H_∞ mixed sensitivity controller (DCC-H_∞ MS controller). The experiment results demonstrate that the proposed controller has a good dynamic performance against parametric uncertainties.

Keywords: Robustness, PWM rectifiers, Dynamic performance, Gap metric.

1. Introduction

Single-phase pulse-width modulation (PWM) rectifiers are widely used in traction systems to replace the traditional transformer with a power electronic transformer. The electric locomotive operates in a dynamic environment where the humidity and temperature have an adverse impact on the electronic transformer. Therefore, robust and reliable control becomes very necessary for electronic devices to ensure the stable and safe operation of a train.

Many control strategies were adopted for single-phase PWM rectifiers, such as proportional integral direct current control (Bahrani et al., 2011), hysteresis control (Liu et al., 2018), proportional resonant (PR), and model predictive control (Song et al., 2015). However, such schemes are sensitive to parameter perturbations. Sliding mode control (Xia et al., 2017) and nonlinear control (Yang et al., 2015) gained considerable popularity. However, these methods are complex and difficult to implement practically.

Robust controllers have been discussed for a variety of applications, including aircraft (Khalil & Fezans, 2021; Azar et al., 2019) and traction systems (Rigatos et al., 2015). These controllers suffer from some limitations namely, their performance is sacrificed in order to gain robustness. The reason is that the parametric uncertainty can only be accounted approximately and then the result gives the impression of being higher than what is being modelled. However, the control strategy is compelled to protect against unrealistic situations that could potentially degrade system performance. Consequently, mixed H_2/H_∞ controller was launched by (Chilali & Gahinet, 1996; Schereer et al., 1997). The mixed H_2/H_∞ controller is also applied to other systems in the literature, such as satellites (Liu et al., 2016), hard-disk drives (Chen et al., 2022), wind turbines (Suinkaew & Ngamroo, 2014), and automobiles (Akcay & Türkay, 2009). The mixed H_2/H_∞ controller gives more freedom of trade-off between robustness and performance in terms of H_2/H_∞ trade-off ratio and pole placement sector location, which enables the controller to deal with many sophisticated scenarios of parametric uncertainties up to the worst-case scenario. The choice of a suitable controller becomes more serious when it is implemented for a device such as a single-phase PWM rectifier, which represents the main device in a traction system.

However, this drew attention to the possibility of using this controller, as no scheme within the scope of this research with application of mixed H_2/H_∞ controller in single-phase PWM rectifiers.

In this paper, a mixed H_2/H_∞ controller is used for direct current control in the presence of inductance variations. The performance of the proposed controller is studied in comparison with that of the H_∞ controller, and further ν-gap metric is used to estimate the level of robustness the proposed controller can provide while maintaining a good dynamic response.

https://doi.org/10.24846/v32i1y202308

The variation in the inductance has a direct effect on the rectifier's direct and quadrature axis currents, particularly the direct axis current; thus, this current will be heavily distorted and may lose reference current tracking if the inductance varies significantly. As a result, an optimal controller is required to achieve current stabilization and adequate reference current tracking. Accordingly, a mixed H_2/H_∞ controller is adopted to handle these two challenges in terms of H_2 optimization and H_∞ optimization. H_2 optimization aims to ensure satisfactory reference tracking, while H_∞ optimization is meant to achieve robust stabilization. The proposed controller is obtained by solving multi-objective optimization problem based on numerical optimization through linear matrix inequalities (LMIs). Despite inductance variations, this can ensure currents have good reference tracking and robust stability.

The remainder of this paper is organized as follows. Section 2 presents the mathematical model of the PWM rectifier. Section 3 deals with the mixed H_2/H_∞ controller design. The experimental results are provided in Section 4, and finally, the conclusion is presented in Section 5.

2. Single-Phase PWM Rectifier Mathematical Model

From Figure 1 based on Kirchoff's voltage law (KVL):

$$L\frac{di_s}{dt} = e_s - Ri_s - u_{ab} \tag{1}$$

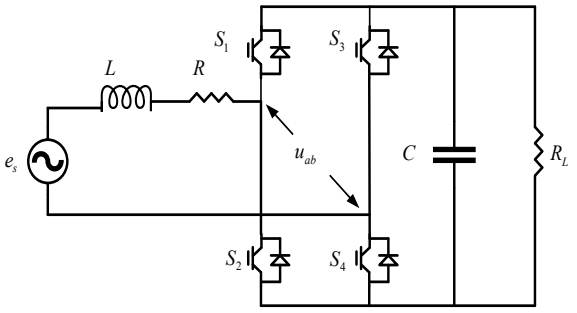

Figure 1. Single-phase PWM rectifier (Adapted from: Song, W., Deng, Z., Wang, S. & Feng, X. (2015) A Simple model predictive control strategy for single-phase PWM converters with modulation function optimization)

In Figure 1 R represents the equivalent resistance of AC-side, R_L is the load resistance and C is the DC-link capacitor. Besides, S_1 to S_4 are active switches. e_s, i_s, $\frac{d}{dt}$ and u_{ab} stand for main alternating voltage, line current, differential operator, and rectifier input voltage, respectively, and e_s and i_s can be defined as follows:

$$e_s = E_{sm}\cos(\omega t) \tag{2}$$

E_{sm} stands for the fundamental peak value of the grid-side voltage. ω represents the fundamental angular frequency.

$$i_s = I_{sm}\cos(\omega t - \varphi) + \sum_{k=3(odd)}^{\infty} I_{smk}\cos(k\omega t - \varphi_k) \tag{3}$$

I_{sm} represents the fundamental peak value of the grid-side current. φ represents the phase difference between the voltage and the current of the grid side. A second-order generalized integrator (SOGI) is used to generate quadrature signals of the voltage and current of the grid. This can be accomplished by the following transfer functions:

$$\begin{aligned} G_\alpha(s) &= \frac{x_\alpha(s)}{x(s)} = \frac{k\omega s}{s^2 + k\omega s + \omega^2} \\ G_\beta(s) &= \frac{x_\beta(s)}{x(s)} = \frac{k\omega^2}{s^2 + k\omega s + \omega^2} \end{aligned} \tag{4}$$

From equation (4), the main alternating voltage e_s and the line current i_s components in the virtual two-axis $(\alpha - \beta)$ reference frame and can be written as:

$$\begin{cases} e_{s\alpha} = e_s = E_{sm}\cos(\omega t) \\ e_{s\beta} = E_{sm}\sin(\omega t) \end{cases} \tag{5}$$

$$\begin{cases} i_{s\alpha} = i_s = I_{sm}\cos(\omega t - \varphi) \\ i_{s\beta} = I_{sm}\sin(\omega t - \varphi) \end{cases} \tag{6}$$

To transform a stationary coordinate into a synchronously rotating coordinate, one can write:

$$\begin{bmatrix} d \\ q \end{bmatrix} = \begin{bmatrix} \cos(\theta) & \sin(\theta) \\ -\sin(\theta) & \cos(\theta) \end{bmatrix} \begin{bmatrix} \alpha \\ \beta \end{bmatrix} \tag{7}$$

$$\begin{bmatrix} \alpha \\ \beta \end{bmatrix} = \begin{bmatrix} \cos(\theta) & -\sin(\theta) \\ \sin(\theta) & \cos(\theta) \end{bmatrix} \begin{bmatrix} d \\ q \end{bmatrix} \tag{8}$$

Equations (5) and (6) can be represented in dq coordinates depending on equation (7) and then substituted in equation (1) to get the following expression:

$$\begin{aligned} e_{sd} &= L\frac{di_{sd}}{dt} + Ri_{sd} - \omega Li_{sq} + u_{abd} \\ e_{sq} &= L\frac{di_{sq}}{dt} + Ri_{sq} + \omega Li_{sd} + u_{abq} \end{aligned} \tag{9}$$

Further, by performing a little arrangement on equation (9) and dividing the entire equation by L, the new mathematical expression will be as follows:

$$\begin{aligned}\frac{di_{sd}}{dt} &= -\frac{R}{L}i_{sd} + \omega i_{sq} + \frac{1}{L}\left(e_{sd} - u_{abd}\right)\\ \frac{di_{sq}}{dt} &= -\frac{R}{L}i_{sq} - \omega i_{sd} + \frac{1}{L}\left(e_{sq} - u_{abq}\right)\end{aligned} \tag{10}$$

By transforming equation (10) into a matrix equation form, one can get the following expression:

$$\begin{bmatrix}\dot{i}_{sd}\\ \dot{i}_{sq}\end{bmatrix} = \begin{bmatrix}-\frac{R}{L} & \omega\\ -\omega & -\frac{R}{L}\end{bmatrix}\begin{bmatrix}i_{sd}\\ i_{sq}\end{bmatrix} + \frac{1}{L}\begin{bmatrix}e_{sd} - u_{abd}\\ e_{sq} - u_{abq}\end{bmatrix} \tag{11}$$

"." in equation (11) indicates the differential operation. With some algebraic manipulation and substitutions, the following expression will be obtained:

$$\begin{bmatrix}\dot{i}_{sd}\\ \dot{i}_{sq}\end{bmatrix} = \begin{bmatrix}-\frac{R}{L} & 0\\ 0 & -\frac{R}{L}\end{bmatrix}\begin{bmatrix}i_{sd}\\ i_{sq}\end{bmatrix} + \begin{bmatrix}\frac{1}{L} & 0\\ 0 & \frac{1}{L}\end{bmatrix}\begin{bmatrix}u_d\\ u_q\end{bmatrix} \tag{12}$$

where:

$$\begin{aligned}u_d &= e_{sd} - u_{abd} + \omega L i_{sq}\\ u_q &= e_{sq} - u_{abq} + \omega L i_{sd}\end{aligned}$$

The output equation is added to the state equation (12) to obtain the complete state space model as follows:

$$\begin{aligned}\begin{bmatrix}\dot{i}_{sd}\\ \dot{i}_{sq}\end{bmatrix} &= \begin{bmatrix}-\frac{R}{L} & 0\\ 0 & -\frac{R}{L}\end{bmatrix}\begin{bmatrix}i_{sd}\\ i_{sq}\end{bmatrix} + \begin{bmatrix}\frac{1}{L} & 0\\ 0 & \frac{1}{L}\end{bmatrix}\begin{bmatrix}u_d\\ u_q\end{bmatrix}\\ y &= \begin{bmatrix}1 & 0\\ 0 & 1\end{bmatrix}\begin{bmatrix}i_{sd}\\ i_{sq}\end{bmatrix} + \begin{bmatrix}0 & 0\\ 0 & 0\end{bmatrix}\begin{bmatrix}u_d\\ u_q\end{bmatrix}\end{aligned} \tag{13}$$

y represents the plant output. From (13) the state matrices can be written as follows:

$$A = \begin{bmatrix}-\frac{R}{L} & 0\\ 0 & -\frac{R}{L}\end{bmatrix}, B = \begin{bmatrix}\frac{1}{L} & 0\\ 0 & \frac{1}{L}\end{bmatrix}$$

$$C = \begin{bmatrix}1 & 0\\ 0 & 1\end{bmatrix}, D = \begin{bmatrix}0 & 0\\ 0 & 0\end{bmatrix}$$

The previous state-space model in (13) can be written as a transfer function as follows:

$$G_{pdq} = C(sI - A)^{-1}B + D \tag{14}$$

The PWM rectifier circuit parameters used in this paper are tabulated in Table 1.

Table 1. PWM Rectifier Parameters

Parameter	Value	Unit
V_s	1550	V
V_{dc}	3000	V
R	0.3	Ohm
L	5.4	mH
C	0.009	F
R_L	25	Ohm

3. Mixed H_2/H_∞ Controller Design

The aim of the current loop control is to maintain the sinusoidal alternating current at the same grid frequency. Thus, the impact of parametric uncertainties must be reduced to achieve this aim. Therefore, it is necessary to design a robust controller capable of handling parametric uncertainties' influence. Figure 2 represents the schematic diagram of the PWM rectifier control system. PLL in Figure 2 represents the phase-locked loop.

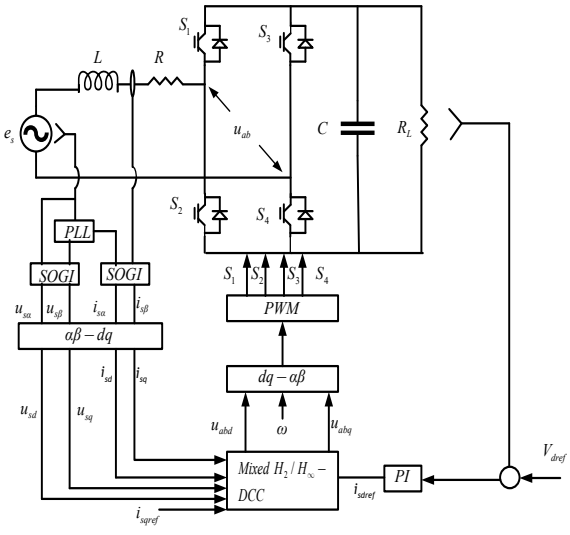

Figure 2. Architecture of the proposed control (Adapted from: Song, W., Deng, Z., Wang, S. & Feng, X. (2015) A Simple model predictive control strategy for single-phase PWM converters with modulation function optimization)

The rectifier's nominal inductance L may change slightly due to temperature, humidity or measurement errors. This change in the inductance should be within permissible bounds; otherwise, it will lead to instability. Therefore, the aim is to obtain a robust controller that achieves nominal performance in terms of good tracking, disturbance attenuation, and robust stability against corresponding perturbations. In other words, the controller will minimize:

$$\min_{K_{dq}} \left\| K_{dq}\left(I + G_{pdq}K_{dq}\right)^{-1} \right\|_2$$

$$\text{Subjected to } \left\| \begin{matrix} \left(I + G_{pdq}K_{dq}\right)^{-1} \\ K_{dq}\left(I + G_{pdq}K_{dq}\right)^{-1} \end{matrix} \right\|_\infty < \gamma$$

γ is a constant smaller than one.

where:

$$G_{pdq} = \left[\begin{array}{cc|cc} -\frac{R}{L} & 0 & \frac{1}{L} & 0 \\ 0 & -\frac{R}{L} & 0 & \frac{1}{L} \\ \hline 1 & 0 & 0 & 0 \\ 0 & 1 & 0 & 0 \end{array}\right]$$

and K_{dq} is the controller in *dq* coordinates.

The goal of multi-objective optimization is to simultaneously minimize the objective 2-norm and ∞-norm:

$$\min_{K_{dq}} \left[\begin{matrix} \left\| K_{dq}\left(I + G_{pdq}K_{dq}\right)^{-1} \right\|_2 \\ \left\| \begin{matrix} \left(I + G_{pdq}K_{dq}\right)^{-1} \\ K_{dq}\left(I + G_{pdq}K_{dq}\right)^{-1} \end{matrix} \right\|_\infty \end{matrix} \right]$$

I in the above expression stands for identity matrix. The optimization problem will be solved numerically using LMIs and the function *h2hinfsyn()* in the LMI toolbox will be used for this purpose.

$\left(I + G_{pdq}K_{dq}\right)^{-1}$ is called sensitivity function and is represented by S_{dq}. $K_{dq}\left(I + G_{pdq}K_{dq}\right)^{-1}$ is called complementary sensitivity function and represented by the symbol T_{dq}

$$K_{dq}(s) = \begin{bmatrix} K_d(s) \\ K_q(s) \end{bmatrix}$$

As shown in Figure 3, which can be redrawn in the well-known feedback control diagram as shown in Figure 4.

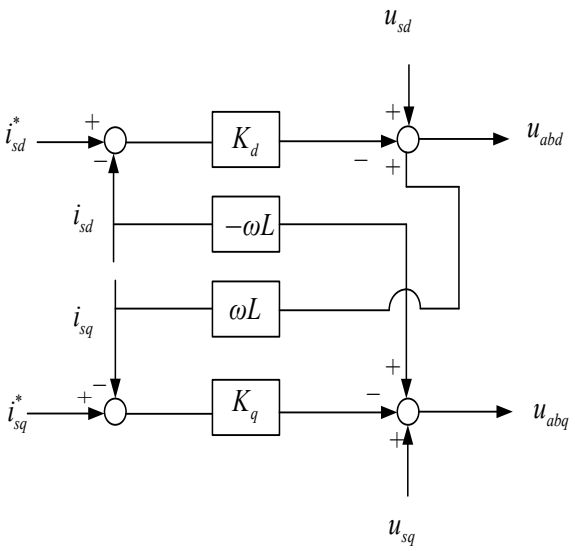

Figure 3. Diagram of the *dq* axis of the current decoupling controller (Adapted from: Peng, L., Ma, L., Liu, H. & Song, W., H_∞ Mixed sensitivity Current Control for Single-Phase PWM Rectifier)

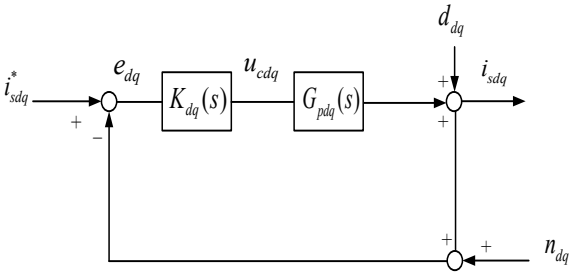

Figure 4. Closed-loop controller diagram of *dq* axis of the current decoupling controller (Adapted from: Zhou, K., A New Approach to Robust and Fault Tolerant Control and from Peng, L., Ma, L., Liu, H. & Song, W., H_∞ Mixed sensitivity Current Control for Single-Phase PWM Rectifier)

$$d_{dq} = \begin{bmatrix} d_d \\ d_q \end{bmatrix}, G_{pdq} = \begin{bmatrix} G_d(s) \\ G_q(s) \end{bmatrix}, n_{dq} = \begin{bmatrix} n_d \\ n_q \end{bmatrix}, e_{dq} = \begin{bmatrix} i^*_{sd} - i_{sd} \\ i^*_{sq} - i_{sq} \end{bmatrix}$$

"*" indicates the reference signals. d_{dq} and n_{dq} are dq axis disturbance and noise, respectively. The weight functions W_1, W_2 and W_3 must be connected as in Figure 5 to get the required performance. W_1 can be expressed as (Beaven et al., 1996; Zhou & Doyle, 1998).

$$W_1 = \frac{s + \omega_1 / M_1}{\varepsilon_1 s + \omega_1}$$

where ε_1, ω_1, M_1 denote the desired steady-state error, bandwidth and peak sensitivity, respectively.

To represent the actuators' amplitude and rate limit constraints, W_2 can be chosen as a constant. In order to improve controller performance, i.e. minimize the steady-state error and reduce overshoot of the response, the weight function W_3 can be expressed as follows:

$$W_3 = \frac{s/M_3 + \omega_3}{s + A\omega_3}$$

where $|K_{dq}S_{dq}(j\omega)| < \frac{1}{|W_3(j\omega)|}$, j represents the imaginary operator.

From Figure 5, w represents the disturbance and y represents the plant output. It is obvious that:

$$\begin{aligned} z_{1\infty} &= W_1 w - W_1 G_{pdq} u \\ z_{2\infty} &= W_2 u \\ z_2 &= W_3 u \\ y &= w - G_{pdq} u \end{aligned} \tag{15}$$

Equation (15) can be written in matrix form as follows:

$$\begin{bmatrix} z_{1\infty} \\ z_{2\infty} \\ z_2 \\ y \end{bmatrix} = \left[\begin{array}{c|c} W_1 & -W_1 G_{pdq} \\ \hline 0 & W_2 \\ \hline 0 & W_3 \\ \hline I & -G_{pdq} \end{array}\right] \begin{bmatrix} w \\ u \end{bmatrix} \tag{16}$$

Matrix equation (16) is expressed in a simplified form by defining new variables as follows:

$$\begin{aligned} z_\infty &= \begin{bmatrix} z_{1\infty} \\ z_{2\infty} \end{bmatrix},\ G_{11} = \begin{bmatrix} W_1 \\ 0 \end{bmatrix} \\ G_{12} &= \begin{bmatrix} -W_1 G_{pdq} \\ W_2 \end{bmatrix},\ G_{21} = 0 \\ G_{22} &= W_3,\ G_{31} = I \\ G_{32} &= -G_{pdq} \end{aligned}$$

Then, based on the previously defined variables, the matrix equation (16) will be simplified as follows:

$$\begin{bmatrix} z_\infty \\ z_2 \\ y \end{bmatrix} = \begin{bmatrix} G_{11} & G_{12} \\ G_{21} & G_{22} \\ G_{31} & G_{32} \end{bmatrix} \begin{bmatrix} w \\ u \end{bmatrix} \tag{17}$$

The main objective of using the above matrix equation is to define the transfer function for the linear fractional transformations (LFTs), namely T_{z2w} and $T_{z\infty w}$.

$$\begin{aligned} T_{z\infty w} &= F_l(G_{dq}, K_{dq}) = G_{11} + G_{12}K_{dq}\left(1 - G_{32}K_{dq}\right)^{-1} G_{31} \\ &= \begin{bmatrix} W_1 \\ 0 \end{bmatrix} + \begin{bmatrix} -W_1 G_{pdq} \\ W_2 \end{bmatrix} K_{dq}\left(I + G_{pdq}K_{dq}\right)^{-1} = \begin{bmatrix} W_1\left(1 + G_{pdq}K_{dq}\right)^{-1} \\ W_2 K_{dq}\left(1 + G_{pdq}K_{dq}\right)^{-1} \end{bmatrix} \\ &= \begin{bmatrix} W_1 S_{dq} \\ W_2 K_{dq} S_{dq} \end{bmatrix} \end{aligned} \tag{18}$$

Similarly, to $T_{z\infty w}$, the expression for T_{z2w} can be derived as follows:

$$\begin{aligned} T_{z2w} &= G_{21} + G_{22}K_{dq}\left(1 - G_{32}K_{dq}\right)^{-1} G_{31} \\ &= 0 + W_3\left(1 + G_{pdq}K_{dq}\right)^{-1} = W_3 K_{dq}\left(1 + G_{pdq}K_{dq}\right)^{-1} \\ &= W_3 K_{dq} S_{dq} \end{aligned} \tag{19}$$

The mixed H_2/H_∞ controller can be obtained by solving the following optimization problem:

$$\min_{K_{dq}} \left\| T_{z2w} \right\|_2$$

Subjected to $\left\| T_{z\infty w} \right\|_\infty < \gamma$

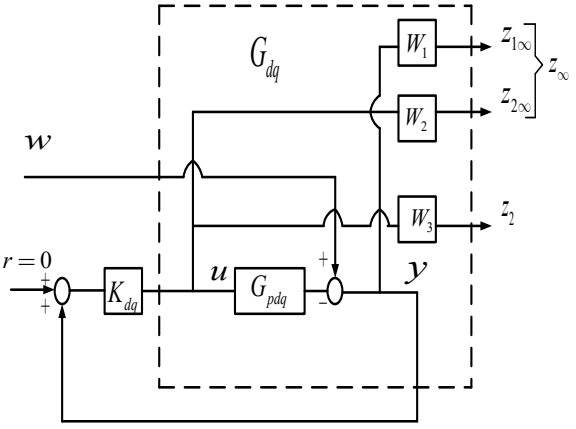

Figure 5. S/KS-T sensitivity optimization (Adapted from: Madoyan, A., Design and Comparison of Mixed H_∞/H_2 Controller for AMB system, Master's thesis)

The block diagram in Figure 5 can be represented as a LFT. Figure 6 below fits in the general LFT framework.

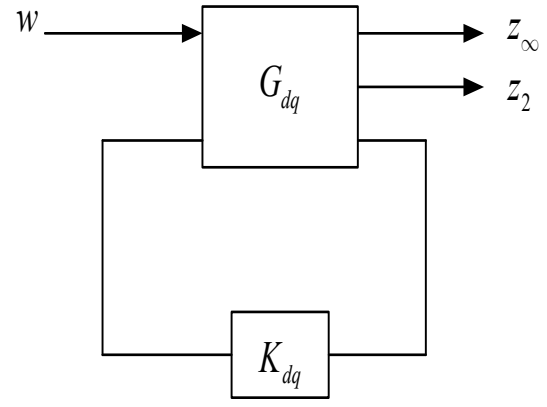

Figure 6. Multi-objective optimization (Adapted from: Ghoreishi, S.A., Nekoui, M. A., Partovi, S. & Basiri, S. O., Application of Genetic Algorithm for Solving Multi-Objective Optimization Problems in Robust Control of Distillation Column)

From Figure 6, the state-space model representation can be expressed as follows:

$$\begin{aligned}\dot{x} &= Ax + B_1 w + B_2 u \\ z_\infty &= C_1 x + D_{11} w + D_{12} u \\ z_2 &= C_2 x + D_{21} w + D_{22} u \\ y &= C_y x + D_y u\end{aligned} \tag{20}$$

The controller has its own dynamics and states in the output feedback. Suppose ξ represents the controller states K_{dq}. Then the state-space equations of the controller can be developed as follows:

$$\begin{aligned}\xi &= A_f \dot{\xi} + B_f y \\ u &= C_f \xi + D_f y\end{aligned} \tag{21}$$

From Figure 6, let the closed-loop transfer function from w to z_∞ be T_∞ and T_2 be a closed-loop transfer function from w to z_2 of plant G_{dq}. Then, the mixed H_2/H_∞ controller problem is to get an output feedback controller $u = K_{dq} y$, u is the output of the controller K_{dq} which stabilizes the plant G_{dq} internally and maintains the following condition:

- $\|T_\infty\|_\infty < \gamma_0$ and $\|T_2\|_2 < \upsilon_0; \gamma_0, \upsilon_0 > 0$
- γ_0, υ_0 are constants smaller than one.
- Minimizes the trade-off ratio criterion
- $\alpha \|T_{z\infty w}\|_\infty^2 + \beta \|T_{z2w}\|_2^2 > 0$ with $\alpha, \beta > 0$

Lemma 1 (H_∞ Performance): (Chilali et al., 1999) T_∞ is the transfer function from w to z_∞-T_∞ RMS does not exceed α if and only if there exists a symmetric matrix X_∞ where:

$$\begin{pmatrix} (A+B_2K)X_\infty + X_\infty(A+B_2K)^T & B_1 \\ B_1^T & -I \\ (C_1+D_{12}K)X_\infty & D_{11} \\ X_\infty(C_1+D_{12}K)^T & \\ D_{11}^T & \\ -\gamma^2 I & \end{pmatrix} < 0$$

Lemma 2 (H_2 Performance): (Chilali et al., 1999) the closed-loop H_2 norm of T_2 does not exceed γ if and only if there exist two symmetric matrices X_2 and Q such:

$$\begin{pmatrix} (A+B_2K)X_2 + X_2(A+B_2K)^T & B_1 \\ B_1^T & -I \end{pmatrix} < 0$$

$$\begin{pmatrix} Q & (C_2+B_{22}K)X_2 \\ X_2(C_2+B_{22}K)^T & X_2 \end{pmatrix} < 0$$

$$Trace(Q) < v^2$$

Solving for Robust Controller

This controller is solved by solving Riccati inequalities through LMIs (Chilali & Gahinet, 1996; Schereer et al., 1997). The mixed H_2/H_∞ robust controller is obtained by the function *h2hinfsyn()* in the LMI toolbox, the controller minimizes mixed H_2/H_∞ trade-off criteria:

$$\alpha \|T_\infty\|_\infty^2 + \beta \|T_2\|_2^2$$

In this study, α = 0.5 and β = 1 which means the controller performance is higher than its robustness. It is worth noting that increasing the value of α can improve robustness, while increasing the value of β can improve dynamic performance. By setting appropriate values for these two parameters, one can find a good balance between performance and robustness. LMI region can be specified by the function *lmireg* it is chosen as a conic sector with an inner angle equal to 3.14 rad and an apex at the origin (Chilali et al., 1999).

The weighting functions are expressed as follows:

$$W_1 = \begin{bmatrix} \dfrac{s+4.804\times10^5}{0.06004s+5285} & 0 \\ 0 & \dfrac{s+4.804\times10^5}{0.06004s+5285} \end{bmatrix}$$

$$W_2 = \begin{bmatrix} 0.5 & 0 \\ 0 & 0.5 \end{bmatrix}$$

$$W_3 = \begin{bmatrix} \dfrac{100s+2.94\times10^7}{s+4.201\times10^7} & 0 \\ 0 & \dfrac{100s+2.94\times10^7}{s+4.201\times10^7} \end{bmatrix}$$

On the other hand, H_∞ controller is synthesized using the same weighting functions as the ones expressed above and the function *hinfsyn()* in the Robust Control Toolbox. The robust controllers will be of a higher order. Therefore, the MATLAB function balred is applied to obtain reduced-order controllers as follows:

Mixed H_2/H_∞ controller:

$$K_{dq} = \begin{bmatrix} K_d & 0 \\ 0 & K_q \end{bmatrix} \tag{22}$$

$$K_{dq} = \begin{bmatrix} \dfrac{0.565s^2+197\times10^4 s+6.756\times10^5}{s^2+8710s+3827} & 0 \\ 0 & \dfrac{0.565s^2+197\times10^4 s+6.756\times10^5}{s^2+8710s+3827} \end{bmatrix}$$

H_∞ controller:

$$K_{dq} = \begin{bmatrix} K_d & 0 \\ 0 & K_q \end{bmatrix} \tag{23}$$

$$K_{dq} = \begin{bmatrix} \dfrac{4.383\times10^4 s+1.185\times10^6}{s^2+2.862\times10^4 s+1.252\times10^4} & 0 \\ 0 & \dfrac{4.383\times10^4 s+1.185\times10^6}{s^2+2.862\times10^4 s+1.252\times10^4} \end{bmatrix}$$

Robust Stability Analysis

The ν-gap metric represents the distance between two plants. It is a good tool for analysing uncertainties and the robustness of feedback systems. Let G and G_Δ be two plants; the ν-gap metric between them is written as follows (Vinnicombe, 1993):

$$\delta_v = \begin{cases} \psi(G,G_\Delta) & \text{if} \begin{cases} \det(I+G_\Delta^* G)\neq 0 \forall \omega \\ \text{wnodet}(I+G_\Delta^* G)+\eta(G) \\ -\eta(G_\Delta)-\eta_0(G_\Delta)=0 \end{cases} \\ 1 & \text{otherwise} \end{cases} \quad (24)$$

where ψ is a function given as follows:

$$\psi(G,G_\Delta)=\left(I+G_\Delta G_\Delta^*\right)^{-1/2}\left(G-G_\Delta\right)\left(I+G^* G\right)^{-1/2} \quad (25)$$

η indicates the number of right half-plane poles (RHP).

$$\left\|\psi(G,G_\Delta)\right\|_\infty = \sup_\omega \bar{\sigma}\left(\psi(G(j\omega),G_\Delta(j\omega)\right) \quad (26)$$

denotes the maximum singular value.

From Figure 7, the stability margin is:

$$b_{G,C} := \begin{cases} \left\|H(G,C)\right\|_\infty^{-1} & \textit{if } [G,C] \textit{ is stable} \\ 0 & \textit{otherwise} \end{cases} \quad (27)$$

where

$$H(G,C)=\begin{bmatrix} I \\ C \end{bmatrix}(I-GC)^{-1}\begin{bmatrix} G & I \end{bmatrix}$$

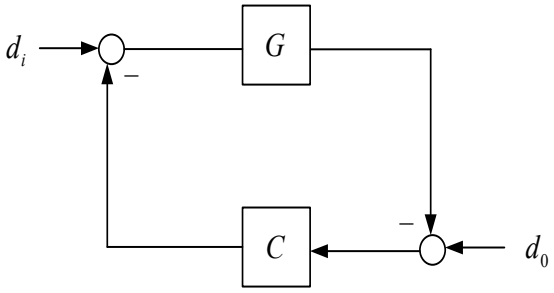

Figure 7. Standard feedback configuration (Adapted from: Vinnicombe, G., Uncertainty and Feedback: H_∞ loop shaping and the v-gap metric)

Theorem 1 (Cantoni & Vinnicombe, 2002)

Let (G_0,C) be stable and $\delta(G_0,G_1)<1$. Then (G_1,C) is stable if

$$b_{G_0,C(\omega)} > \psi(G_0(j\omega),G_1(j\omega)), \forall\omega$$

$b_{G_0,C}(\omega)$ and $\psi(G_0(j\omega),G_1(j\omega))$ are defined as follows:

$$\frac{1}{b_{G_0,C(\omega)}} := \bar{\sigma}\left(\begin{bmatrix} I \\ C(j\omega) \end{bmatrix}(I-G(j\omega)C(j\omega))^{-1}\begin{bmatrix} G(j\omega) & I \end{bmatrix}\right) \quad (28)$$

$$\psi(G_0(j\omega),G_1(j\omega)) := \bar{\sigma}(\psi(G_0(j\omega),G_1(j\omega)) \quad (29)$$

and

$$\psi(G_0(j\omega),G_1(j\omega)) := (1+G_1(j\omega)G_0(j\omega))^{1/2}(G_0(j\omega) - G_1(j\omega))(I+G_1(j\omega)G_0(j\omega))^{-1/2} \quad (30)$$

4. Experimental Results

Figure 8 illustrates the hardware-in-loop experimental platform, which consists of a dSPACE real-time simulator, a DSP TMS320F28335 control board, an oscilloscope, and two computers as an information interface. The rectifier topology is configured in the dSPACE simulator. The voltage and current received by the DSP board from the interface board will be sent to the pulse-width modulation (PWM) signals.

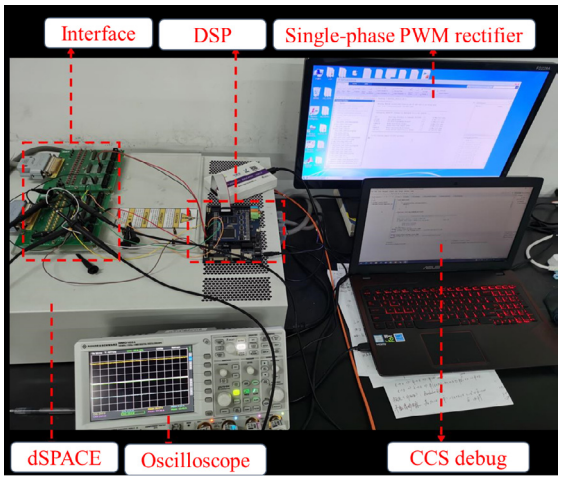

Figure 8. Hardware-in-loop experimental platform

From Theorem 1, it is obvious that the system will be stable if the ν-gap metric produced by the inductance variation is lower than the stability margin; otherwise, the system will be unstable, as indicated in Figure 9.

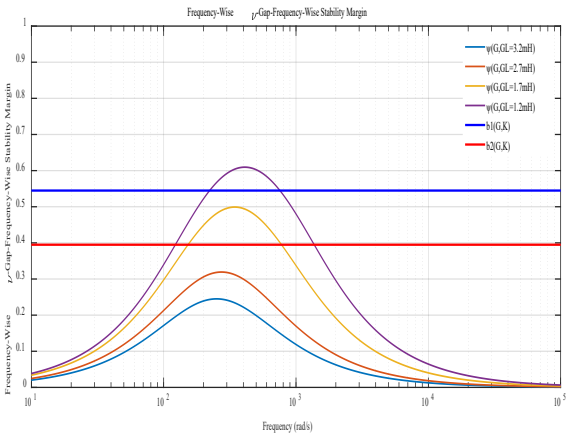

Figure 9. ν-gap metric and stability margin frequency response

From Figure 10, it is obvious that both controllers achieved pure sinusoidal waveforms under normal operation conditions.

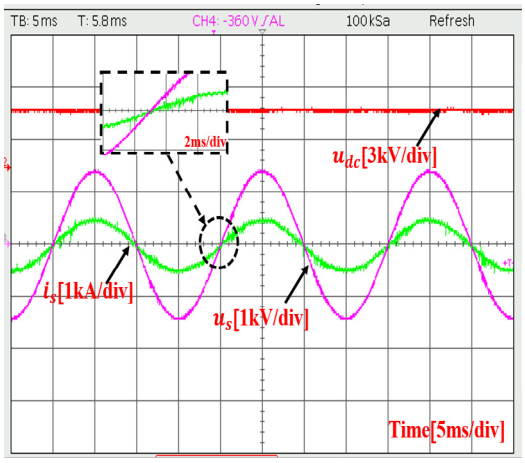

(a)

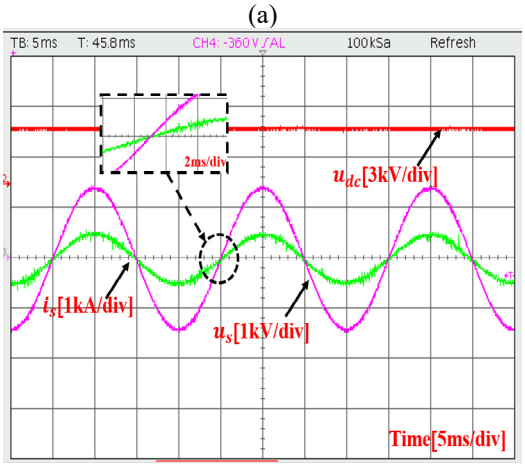

(b)

Figure 10. Experimental waveforms of AC current and voltage, and DC-link voltage (a) DCC-based mixed H_2/H_∞ controller; (b) DCC-based H_∞ MS controller

Figure 11 demonstrates that mixed H_2/H_∞ controller performs better than H_∞ MS controller in terms of percentage overshoot and settling time when the rectifier operates with the nominal parameters.

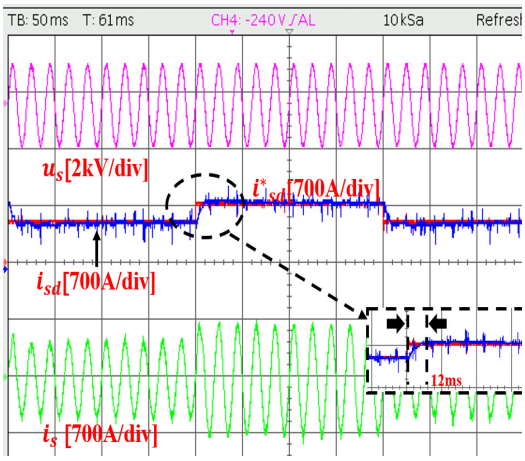

(a)

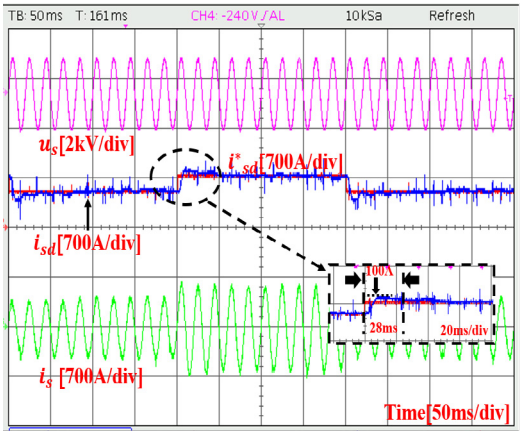

(b)

Figure 11. Experimental waveforms of $u_s, i_{sd}, i^*_{sd}, i_s$ with the nominal parameters (a) DCC-based mixed H_2/H_∞ controller; (b) DCC-based H_∞ MS controller

According to Figures 12 and 13, mixed H_2/H_∞ controller in both circumstances outperforms H_∞ mixed sensitivity (MS) controller by achieving a quicker settling time and no percentage overshoot. This situation is accomplished when the inductance is reduced to 3.2mH and 2.7mH, respectively.

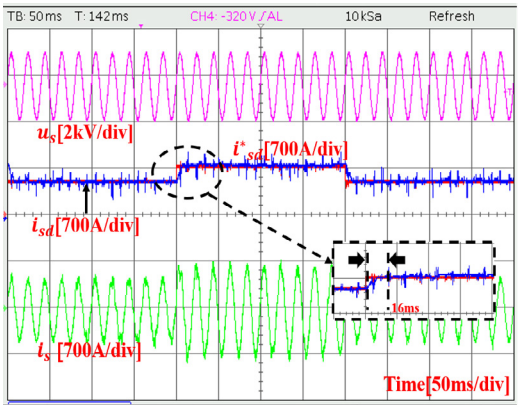

(a)

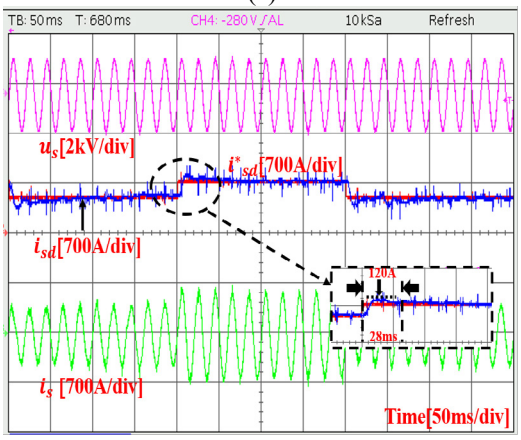

(b)

Figure 12. Experimental waveforms of $u_s, i_{sd}, i^*_{sd}, i_s$ when the inductance L=3.2mH (a) DCC-based mixed H_2/H_∞ controller; (b) DCC-based H_∞ MS controller

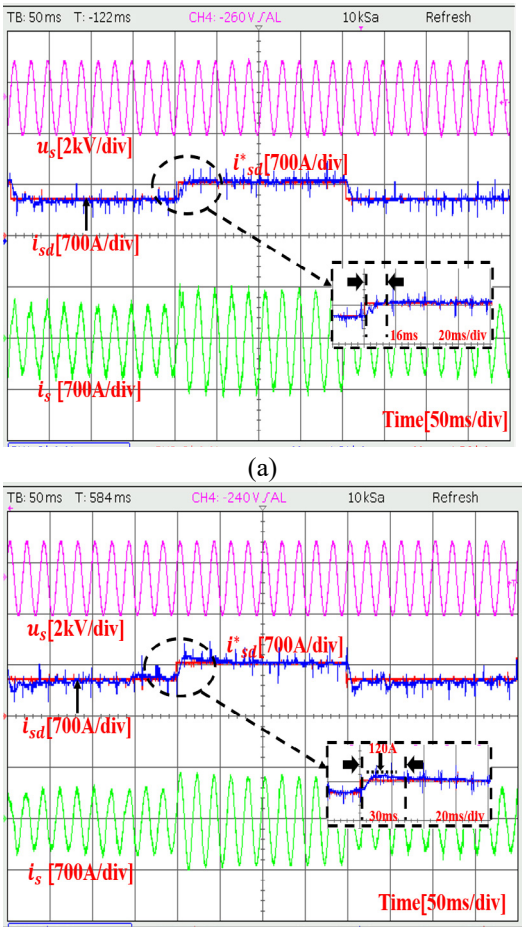

Figure 13. Experimental waveforms of $u_s, i_{sd}, i^*_{sd}, i_s$ when the inductance L=2.7mH (a) DCC-based mixed H_2/H_∞ controller; (b) DCC-based H_∞ MS controller

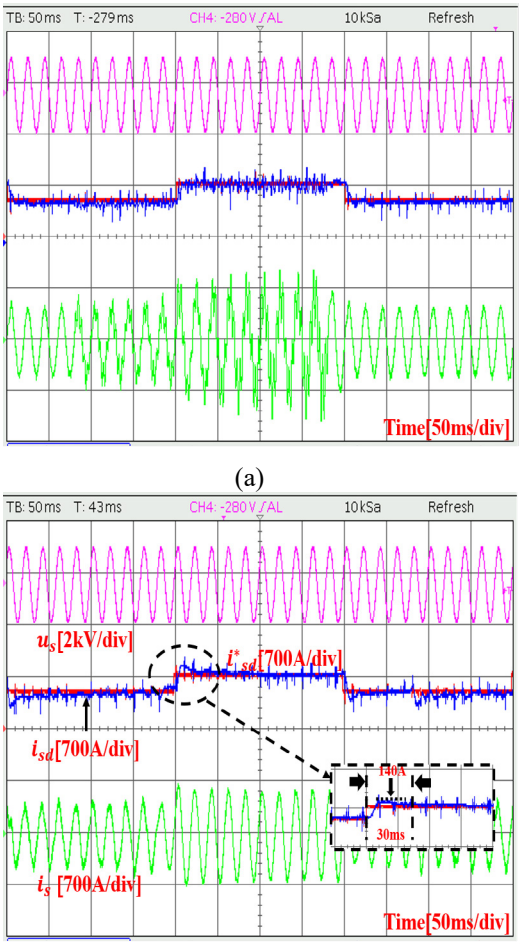

Figure 14. Experimental waveforms of $u_s, i_{sd}, i^*_{sd}, i_s$ when the inductance L=1.7mH (a) DCC-based mixed H_2/H_∞ controller; (b) DCC-based H_∞ MS controller

Both controllers can stabilize the rectifier in both cases because the stability margins of both controllers are greater than the ν-gap, which is obvious in Figure 9. The comparison between the two controllers in terms of settling time and percentage overshoot for different inductances is shown in Table 2.

From Figure 14, it can be noted that H_∞ MS controller is able to stabilize the system when the inductance is reduced to 1.7mH but with the mixed H_2/H_∞ controller, the system loses stability because the ν-gap exceeds the stability margin.

However, the H_∞ MS controller loses its robustness when the inductance is further reduced to 1.2mH as illustrated in Figure 15. Mixed H_2/H_∞ controller is the best among the robust controllers because it achieves both robustness and dynamic performance at the same time, and the stability margin of this controller can always be improved by choosing an appropriate trade-off ratio between H_∞ and H_2.

Table 2. Controller Comparison-Summary

	Mixed H_2/H_∞ Controller		**H_∞ Controller**	
Case	**Percentage overshoot**	**Settling time**	**Percentage overshoot**	**Settling time**
Nominal Parameters	-	12 msec	14.3%	28 msec
L=3.2mH	-	16 msec	17.1%	28 msec
L=2.7mH	-	16 msec	17.1%	30 msec
L=1.7mH	Unstable signals		Stable signals	
L=1.2mH	Unstable signals		Unstable signals	

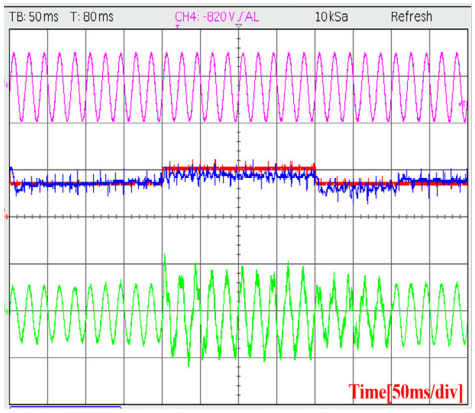

Figure 15. Experimental waveforms of $u_s, i_{sd}, i_{sd}^*, i_s$ when the inductance L=1.2mH DCC-based H_∞ MS controller

5. Conclusion

In this paper the properties of H_2 and H_∞ robust control techniques are combined in the mixed H_2/H_∞ controller which is applied to a single-phase PWM rectifier. The analysis of parametric uncertainty and of the robustness of feedback systems has been performed using ν-gap metric. The experimental results demonstrated a decent dynamic performance of the proposed controller in the context of inductance fluctuations and a good degree of robustness via ν-gap metric. The results are promising and future research could focus on analysing the controller effectiveness in the existence of sensor faults.

REFERENCES

Akcay, H. & Türkay, S. (2009) Influence of tire damping on mixed H_2/H_∞ synthesis of half-car active suspension. *Journal of Sound and Vibration*. 322(1-2), 15-28.

Azar, A. T., Serrano F. E., Hameed, I. A.,Kamal, N. A. & Vaidyanathan, S. (2019) Robust H-infinity decentralized control for industrial cooperative robots. In: *Proceedings of the 5th International Conference on Advanced Intelligent Systems and Informatics, October 26-28, 2019, Cairo, Egypt.* Springer. pp. 254-265.

Beaven, R. W., Wright, M. T. & Seaward, D. R. (1996) Weighting function selection in the H_∞ design process. *Control Engineering Practice.* 4, 625-633. doi: 10.1016/0967-0661(96)00044-5.

Bahrani, B., Ruffer, A. & Kenzelmann, S. (2011) Vector control of single-phase voltage-source converters based on fictive-axis emulation. *IEEE Transactions on Industry Applications.* 47(2), 831-840. doi: 10.1109/TIA.2010.2101992.

Chen, Z., Shah, P. & Horowitz, R. (2022) Head-Positioning Control in Triple-Stage-Actuator Enterprise Hard Disk Drives Using Mixed H_2/H_∞ Synthesis Methodologies. *ASME Letters in dynamic Systems and Control.* 2(1), 1-8.

Cantoni, M. & Vinnicombe, G. (2002) Linear feedback systems and the graph topology. *IEEE Transactions on Automatic Control,* 47(5), 710-719.

Chilali, M., Gahinet, P. & Apkarian, P. (1999) Robust pole placement in LMI regions. IEEE Transactions on Automatic Control, 44(12), 2257-2270.

Chilali, M. & Gahinet, P. (1996) H_∞ design with pole placement constrains: an LMI approach. *IEEE Transactions on Automatic Control.* 41, 358-367. doi: 10.1109/9.486637.

Khalil, A. K. & Fezans, N. (2021) A multi-channel H-infinity preview control approach to load alleviation design for flexible aircraft. *CEAS Aeronautical Journal*. 401-412. doi: 10.1007/s13272-021-00503-z.

Liu, C., Sun, Z. W., Shi, K. K. & Wang, F. (2016) Mixed *H2/H∞* Control approach and its application in satellite control system. *International Journal of Engineering Research in Africa.* 25, 89-97. DOI: 10.4028/www.scientific.net/JERA.25.89.

Liu, B., Song, W., Ma, J., Feng, X. & Li, W. (2018) Dynamic performance improvement of single-phase PWM converters with power hysteresis control scheme. *IET Power Electronics.* 11(12), 1894-1902. doi: 10.1049/iet-pel.2017.0624.

Rigatos, G., Siano, P., Wira, P. & Profumo, F. (2015) Nonlinear H-infinity feedback control for asynchronous motors of electric trains. *Intelligent Industrial Systems*. 1, 85-98. doi: 10.1007/s40903-015-0020-y.

Surinkaew, T. & Ngamroo, I. (2014) Robust power oscillation damper design for DFIG-based wind turbine based on specified structure mixed H_2/H_∞ control. *Renewable Energy.* 66, 15-24. doi: 10.1016/j.renene.2013.11.060.

Schereer, C., Gahinet, P. & Chilali, M. (1997) Multiobjective output-feedback control via LMI optimization. *IEEE Transactions on Automatic Control.* 42(7), 896-911. doi: 10.1109/9.599969.

Song, W., Deng, Z., Wang, S. & Feng, X. (2015) A Simple model predictive control strategy for single-phase PWM converters with modulation function optimization. *IEEE Transactions on Power Electronics.* 31(7), 5279-5289. doi: 10.1109/TPEL.2015.2481323.

Vinnicombe, G. (1993) Frequency domain uncertainty and the graph topology. *IEEE Transactions on Automatic Control.* 38(9), 1371-1383.

Xia, J. Guo, Y., Dai, B. & Zhang, X. (2017) Sensor fault diagnosis and system reconfiguration approach for an electric traction PWM rectifier based on sliding mode observer. *IEEE Transactions on Industry Applications.* 53(5), 4768-4778. doi: 10.1109/TIA.2017.2715816.

Yang, J. & Shi, W. (2015) Nonlinear control strategy for direct AC current control in single-phase PWM rectifier. *Power System Protection and Control*. 20, 114-118.

Zhou, K. and Doyle, J. C. (1998) *Essentials of robust control.* Upper Saddle River, New Jersey, Prentice Hall.